Russian Journal of Earth Sciences

The Use of Landsat 8 in Detecting Potential Mineral Zones in West Nusa Tenggara, Indonesia

U. A. Said[*,1], **R. A. Bantan**[1], **A. A. Mannaa**[1], **and Y. Taufiq**[2]

[1] Department of Marine Geology, Faculty of Marine Sciences, King AbdulAziz University, Jeddah, Saudi Arabia
[2] PT. Sumbawa Timur Mining, Jakarta, Indonesia
* **Correspondence to:** Umar Abdulrahim Said, usaid@stu.kau.edu.sa

Abstract: The remote sensing analysis within the Hu'u District area is known to face a challenge with dense vegetation. The problem affects the accurate reading of spectral reflectance from satellites, influencing the differentiation between potential mineral zones and vegetation. Therefore, this study aims to carry out a remote sensing analysis of densely vegetated areas to differentiate minerals from vegetation and obtain potential mineral zones. The combination band ratios and principal component analysis (PCA) methods are used to acquire potential mineral zones. Furthermore, Landsat 8 images freely available on Google Earth Engine are adopted and the validation is carried out using a drill hole from previous study. The results show that band ratios method cannot distinguish mineral zones from vegetation. However, PCA method can recognize potential mineral zones. This is the result from PCA method with band combination of bands 1, 2, 3, 4, 5, and 6 as the first group and band 2, 4, 5, and 6 as the second group.

Keywords: Landsat 8, Band Ratio, Principal Component Analysis, Mineral, Densely Vegetated Areas.

Citation: Said, U. A., R. A. Bantan, A. A. Mannaa, and Y. Taufiq (2024), The Use of Landsat 8 in Detecting Potential Mineral Zones in West Nusa Tenggara, Indonesia, *Russian Journal of Earth Sciences*, 24, ES5010, EDN: HSCGRG, https://doi.org/10.2205/2024es000921

1. Introduction

Geological mapping is perceived as an indispensable component across different disciplines and applications. In this context, remote sensing datasets have been developed as a cost-effective, efficacious, as well as temporally and labor-efficient methodology, particularly when subjected to traditional approaches of field mapping. Landsat data has also been extensively deployed for tasks such as discriminating among rock units, deciphering lineaments, and showing hydrothermal alterations. Due to economic concerns, mineral mapping using satellite data speeds up exploration, lowers expenses, as well as accurately and quickly identifies broad regions [*Aita and Omar*, 2021; *Bakardjiev and Popov*, 2015; *Hede et al.*, 2015; *Shebl and Csámer*, 2021].

Optical appraisal of aerial pictures has been leveraged to correctly show these formations, particularly linear structures or lineaments. In the present era, with the advent of Geographic Information System (GIS) expertise, the high-resolution data gained from photos, autonomous parsing of satellite images, and Landsat, is strongly propagated [*Takodjou Wambo et al.*, 2016]. Alteration mineral indices such as the OH-bearing, pyrophyllite, kaolinite, alunite, and calcite were established by detecting argillic, phyllic, and propylitic alternations in epithermal deposit and porphyry copper deposit using Landsat 8 [*Ombiro et al.*, 2021; *Parcutela et al.*, 2022; *Shim et al.*, 2021; *Zhang et al.*, 2016]).

Several studies have focused on methodologies to show geological structures by taking advantage of Principal Component Analysis (PCA) and Band Ratio (BR) among other techniques. The use of the conventional PCA approach may substantially enhance the precision of geological mapping, facilitating a more accurate identification and interpretation of geospatial and spectral data [*Carranza and Hale*, 2002; *Chen et al.*, 2021; *Ghasemi et al.*, 2018].

Research Article

Received: 21 March 2024
Accepted: 29 July 2024
Published: 24 December 2024

2. Study Area

The study area is located within the Hu'u district, Dompu Regency on Sumbawa Island, situated in West Nusa Tenggara, Indonesia, as seen in Figure 1. It forms a portion of the territory 50 under projects managed by PT Sumbawa Timur Mining (PT STM). Within the district, there exist three principal porphyry Cu-Au prospects, specifically the Humpa Leu East, Sori Hiu, and Onto prospects [*Fadlin et al.*, 2023]. The district has been hypothesized to be a paleovolcano, characterized by Upper Miocene Basaltic Andesite lava, with radiometric dating at an age of 5 ± 0.2 Ma years. Regionally, the rock formations are categorized as constituents of the Old Volcanics Rocks Formation [*Verdiansyah et al.*, 2023]. The Hu'u intricate features various surface possibilities, manifested as a lithocap of widespread epithermal-style alteration but some are connected to a porphyry situated underneath the ground [*Verdiansyah et al.*, 2021].

The Hu'u project region is situated at the junction of many significant fault zones, according to a seismotectonic assessment. A significant sinistral fault with an NW trend is projected across the region from the southwest face of the Tambora volcano. Furthermore, a significant dextral fault with an NE trend extends along the bay straight west of the Hu'u region [*Burrows et al.*, 2020].

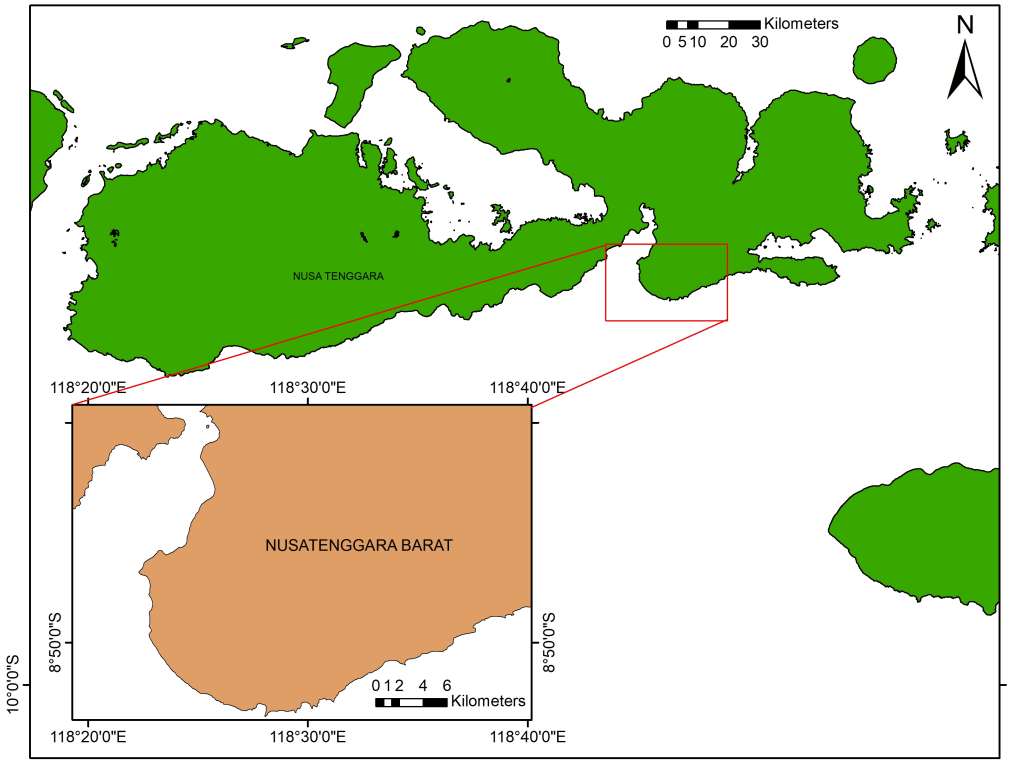

Figure 1. Hu'u District, West Nusa Tenggara, Indonesia as the study area.

3. Method

3.1. Images Data

The visible and shortwave bands of the Landsat 8 image were thought to be useful for identifying the type of mineral based on its spectral signature or spectral reflection properties [*Setianto et al.*, 2021].

Landsat 8 data used is freely obtained from Google Earth Engine as a compilation of images from April 2013 to 2023. This data is pre-configured in a Top of Atmosphere (TOA) format after radiometric and geometric corrections. Furthermore, cloud cover filter is the preprocessing conducted to obtain the least cloudy images. The purpose of the

pre-processing is to derive a collection of satellite images, spanning several years, with minimal cloud interference.

This study made use of Landsat 8 satellite images, which has a range of spectral bands capturing multiple wavelengths of light. These electromagnetic spectrum bands span the visible and shortwave infrared regions. Specifically:

- Band 2 (Blue: 0.45–0.51 μm): This band's ability to penetrate clear water makes it useful for mapping underwater structures and evaluating bodies of water.
- Band 3 (Green: 0.53–0.59 μm): Useful for assessing the health and vigor of vegetation, as it captures the green reflectance peak from chlorophyll.
- Band 4 (Red: 0.64–0.67 μm): This band is crucial for distinguishing between vegetation and bare soil, as healthy vegetation absorbs red light.
- Band 5 (Near Infrared, NIR: 0.85–0.88 μm): Highly reflective in vegetation, this band is used for assessing biomass content and mapping vegetation.
- Band 6 (Shortwave Infrared 1, SWIR1: 1.57–1.65 μm): Sensitive to moisture content, useful in studying soil and vegetation water content.
- Band 7 (Shortwave Infrared 2, SWIR2: 2.11–2.29 μm): Effective for detecting hydrothermal alterations in rocks and distinguishing between different types of minerals.

Understanding these spectral characteristics is fundamental for accurately interpreting the satellite imagery and applying subsequent analysis techniques

3.2. Pre-Processing

The data, procured from the Google Earth Engine, originates from Landsat 8, Collection 2, Tier 1. This data is pre-configured in a TOA format after radiometric and geometric corrections. In addition, the pre-processing is to derive a collection of satellite images, spanning several years, with minimal cloud interference. Obtaining raw Landsat satellite images in the region of interest is crucial in providing the conditions in the targeted area.

3.3. Band Ratio

Band rationing is a technique where one band's Digital Number (DN) is split by the value of a different band's DN. When pointing out elements or materials that are not visible in the raw bands, band ratios can potentially be beneficial. It consists of applying numerical methods to multispectral pictures to lessen spectral reflectance fluctuations brought on by topography or fluctuations in sunlight illumination angle and to derive certain spectral responses [*Ghasemi et al.*, 2018].

Band combinations tested in this study are 4/2, 6/7, 6/5, and 7/5 to obtain iron oxide, hydroxyl-bearing rocks, ferrous minerals, and clay, respectively.

3.4. Band Ratio Composites

The 3 combinations of band ratio composites experienced in the project are Sabin's ratio, Kaufmann's ratio, and composite of 4/2, 6/7, and 5. Sabin's ratio is expected to define a hydrothermal alteration map, while Kaufmanns' ratio is anticipated to distinguish altered rocks and lithological elements from the vegetation. The composites of 4/2, 6/7, and 5 are used to differentiate altered rocks and outcrops from trees and plants.

3.5. PCA

To mitigate and dissociate the inaccurate impacts of flora in mapping hydrothermal alterations and revealing the lithology of tropical terrain, the Principal Components Analysis (PCA) is employed [*Pour and Hashim*, 2014]. In areas of dense vegetation, pixels may exclusively depict vegetation spectra, while in less densely vegetated regions with insufficient spatial resolution pixels, they may represent a mix of different materials. Techniques for detecting and mapping hydrothermally altered rocks typically aim to substantially separate or reduce the spectral impact of vegetation from that of the underlying substrate. The software defoliant technique, an image enhancement method, employs a prime components analysis of two band ratios that emphasize the effects of the objective interest, with

input band ratio images chosen based on their information associated to components of concentration (e.g., hydrothermal alteration) and their interference from other components such as vegetation. This method elucidates variance due to spectral response similarities and highlights unique contributions from each component [*Ghasemi et al.*, 2018].

There are two combinations of bands for PCA. The group of bands 1, 2, 3, 4, 5, and 6, as well as those from bands 2, 4, 5 and 6. Eigenvalue and eigenvector are required to calculate visualization in RGB format.

4. Results

4.1. Raw Landsat Satellite Images

The true color composite requires the visual combinations of bands 2, 3, and 4 from Landsat 8 satellite. The image area should have a low cover of clouds to disturb the reflectance of signal from a satellite. The cloud covering is inversely proportional to the accuracy of the results. From Figure 2, the region of interest can be known as a densely vegetated area, disturbing the reflectance of signal from a satellite. Meanwhile, the signal reads the vegetation instead of mineral and an advanced analysis is essential to obtain the reflection of mineral under tight vegetation. Figure 2 is a compilation of Landsat 8 images from April 2013 to 2023 freely available and obtained from Google Earth Engine showing true color composite.

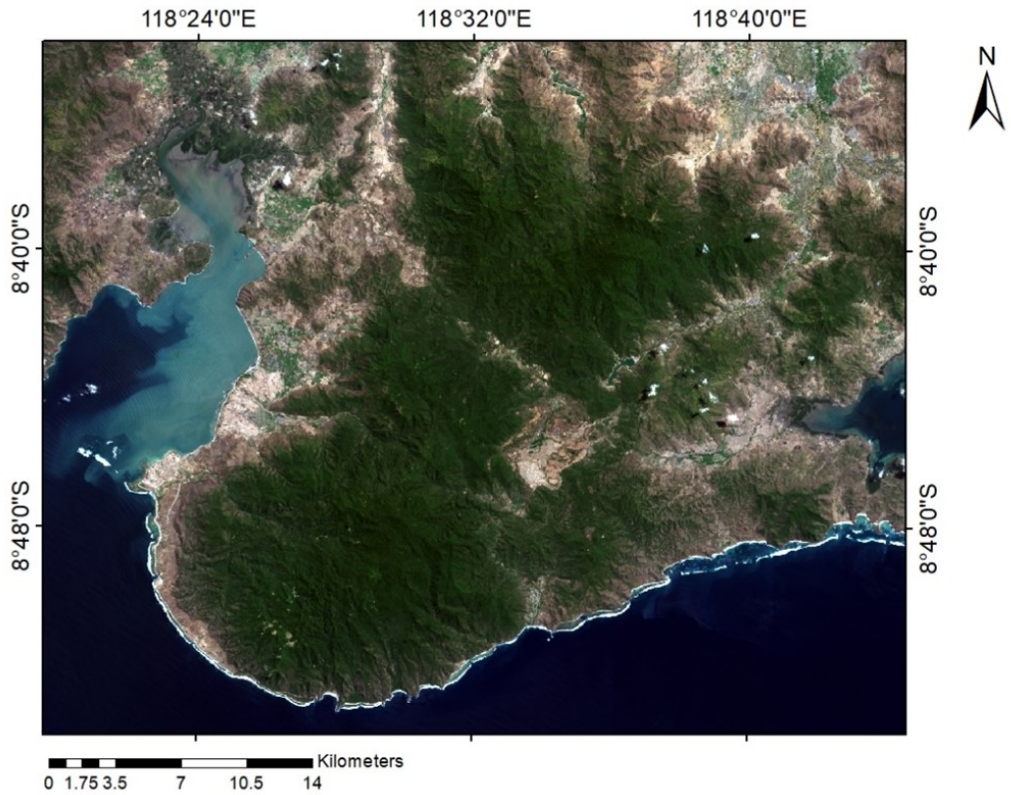

Figure 2. True color composites are presented by bands 2, 3, and 4 to explain the real condition of the study area with the least clouds.

4.2. Band Ratios

Figure 3A, 3B, 3C, and 3D shows the results of band 4/2, 6/7, 6/5, and 7/5, respectively. Mineral potential zone is not reported due to vegetation and the expected result is unachieved by combining some bands. Therefore, this method does not apply to the study area due to increased vegetation.

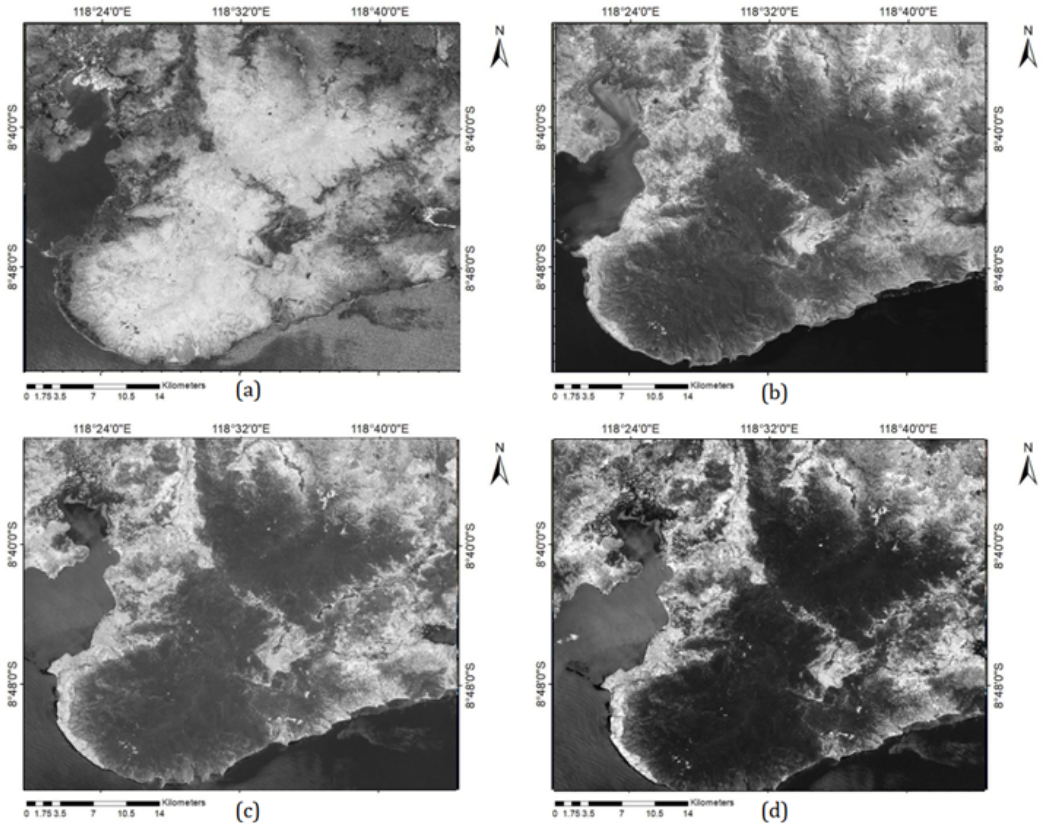

Figure 3. (a) Band ratio 4/2, (b) Band Ratio 6/7, (c) Band Ratio 6/5, (d) Band Ratio 7/5. These combinations were conducted to detect potential zones.

4.3. Band Ratio Composites

Sabin's ratio is expected to define the hydrothermal alteration map by combining bands 4/2, 6/7, and 6/5. Kaufmanns' ratio is anticipated to distinguish altered rocks and lithological units from the flora using a combination of 7/5, 5/4, and 6/7. Meanwhile, composites of 4/2, 6/7, and 5 are optimized to differentiate altered rocks and outcrops from woodlands. Figures 4A, 4B and 4C present the result of Sabin's ratio, Kaufmann's ratio, and a composite of 4/2, 6/7, and 5. These three composites cannot identify potential mineral zones and the vegetation is still the unworked factor. Even though the three bands are tested in one composite of RGB format, the expected result is not attained.

4.4. PCA

The first combination group consists of bands 1, 2, 3, 4, 5, and 6 to recognize hydrothermally altered rocks and other minerals from trees. In addition, the second group of bands 2, 4, 5, and 6 are processed to obtain iron oxides from plants.

Table 1 shows that PC1, PC2, and PC3 account for 99.83% of the variation to create the RGB composite for producing the primary component seen in Figure 5a. According to the illustration, the green and blue colors symbolize flora and rocks subjected to hydrothermal alteration, respectively.

PC4 comprises 0.09% of the variance data and has the greatest loading positive and negative Eigenvector values of 0.779882 and −0.612408 for bands 2 and 4, respectively. In broad terms, minerals related to iron oxides show low absorption and reflectance between and 0.45–0.51 μm, respectively. Therefore, regions connected to iron oxides in bands 2 and 4 are bright in the PC4 picture.

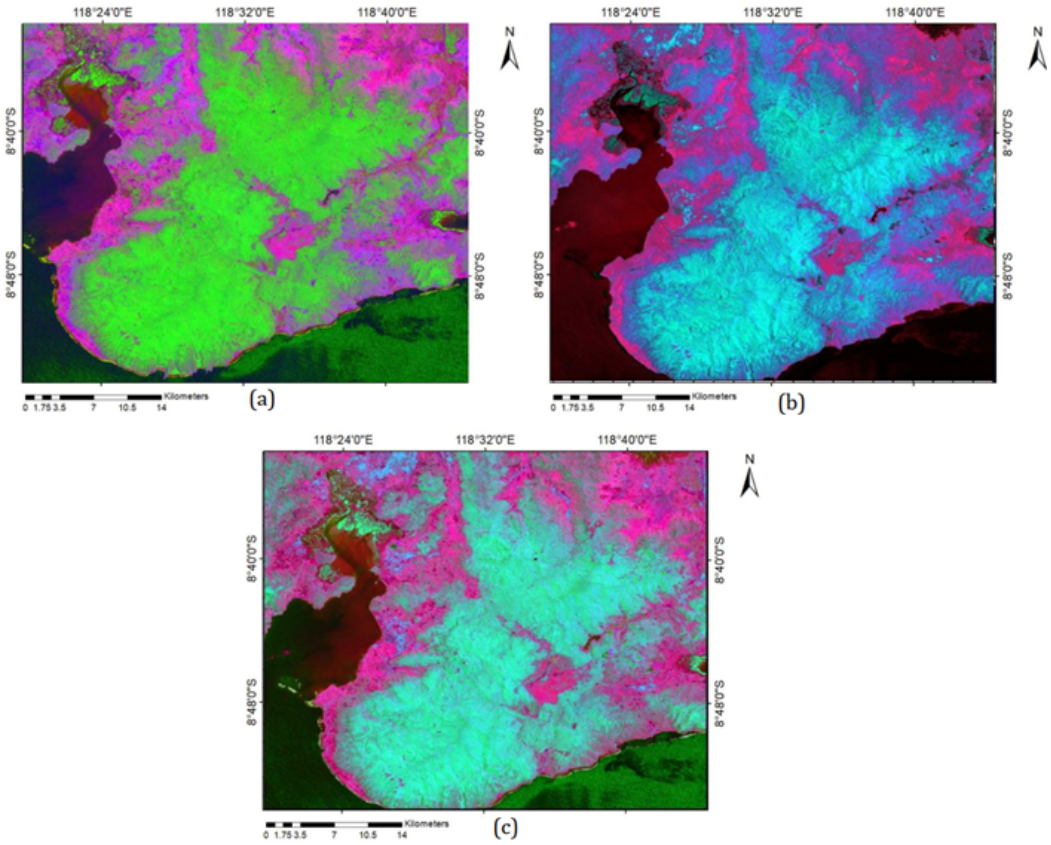

Figure 4. A) Sabin's Ratio (band 4/2, 6/7, and 6/5), B) Kaufmann's Ratio (band 7/5, 5/4, 6/7), C) Composite of 4/2, 6/7, 5.

Table 1. Eigen Values and Eigen Vectors for Bands 1, 2, 3, 4, 5 and 6

	PC1	PC2	PC3	PC4	PC5	PC6
Band 1	0.020360	0.192974	−0.334840	−0.494944	0.402861	0.665554
Band 2	0.035911	0.238785	−0.402445	−0.452621	0.201009	−0.731068
Band 3	0.103666	0.253710	−0.484258	−0.032229	−0.816609	0.149964
Band 4	0.155918	0.433000	−0.377308	0.723144	0.350531	0.005456
Band 5	0.754882	−0.595431	−0.265794	0.023034	0.066237	−0.007135
Band 6	0.627209	0.547126	0.527643	−0.160181	−0.056473	0.002697
Eigen Values	0.026078	0.004487	0.001089	0.000040	0.000011	0.000001
Percentage of Eigen Values	82.251%	14.151%	3.436%	0.126%	0.035%	0.002%
Cumulative Percentage of Eigen Values	82.251%	96.402%	99.837%	99.963%	99.998%	100.000%

Figure 5a explains that potential mineral zones are depicted in dark blue, while vegetation is shown in green. In this context, the bright pixels represent hydrothermally altered rocks in Figure 5b.

The drill hole data and boundaries of the company's project area used are presented in Figure 6. The white lines and yellow dots represent the project area boundaries and drill hole locations, respectively. From Figure 7, the locations of the drill holes are matched with the blue areas from the analysis representing potential mineral zones. Therefore, the green squares can be potential areas for upcoming exploration projects.

Table 2. Eigen Eigen Values and Eigen Vectors for Bands 2, 4, 5, and 6

	PC1	PC2	PC3	PC4
Band 2	−0.033644	0.223736	0.583605	0.779882
Band 4	−0.153175	0.432613	0.643692	−0.612408
Band 5	−0.761896	−0.611333	0.213294	−0.017100
Band 6	−0.628427	0.623747	−0.446734	0.128249
Eigen Values	0.025795	0.004078	0.000661	0.000027
Percentage of Eigen Values	84.40%	13.35%	2.16%	0.09%
Cumulative Percentage of Eigen Values	84.40%	97.75%	99.91%	100.00%

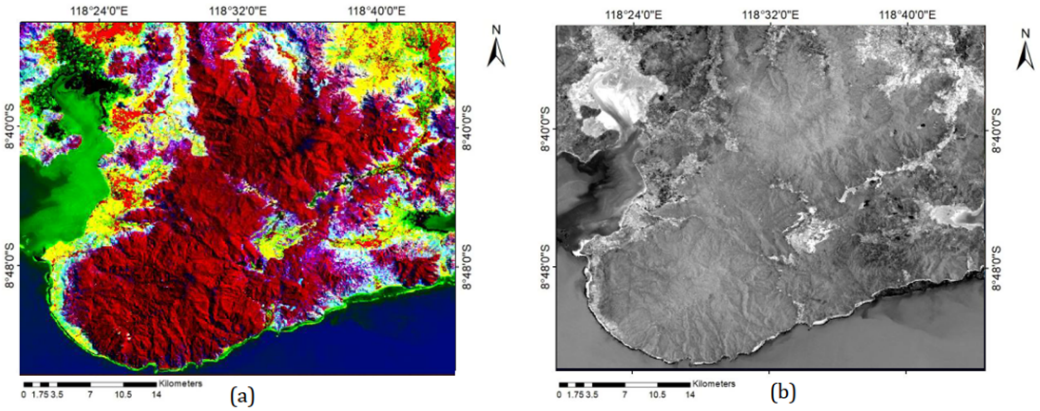

Figure 5. A) The PC1, PC2, and PC3 components in RGB combination. Potential mineral zones are illustrated in dark blue. B) Principal component 4 (PC4). The bright pixels correspond to hydrothermally altered rocks.

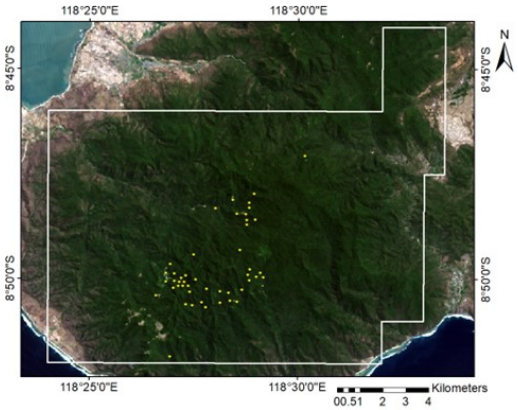

Figure 6. Drill hole locations (modified after [*Burrows et al.*, 2020]). The yellow dots and white lines are drill holes and project boundaries, respectively.

5. Discussion and Conclusion

The true color composite was reported to require the visual combinations of bands 2, 3, and 4 from Landsat 8 satellite. The image area had minimal cloud cover, reducing the potential for cloud to interfere with the satellite signal's reflectance. The clouds covering was inversely proportional to the accuracy of the results and the region of interest could be known as a densely vegetated area. In this context, the vegetation disturbed the reflectance

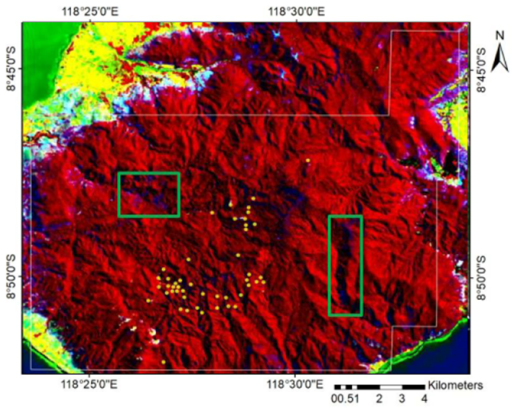

Figure 7. Validated map. Yellow dots are drill holes. Dark blue are potential mineral zone. The green boxes are the suggested next exploration areas.

of the signal from a satellite. Therefore, an advanced analysis is essential to obtain the reflection of minerals under tight vegetation.

Band ratios 4/2, 6/7, 6/5, and 7/5 were tested as visualized in Figure 3 but could not differentiate mineral potential zone. The vegetation disturbed the satellite signal reflectance and the expected result could not be accomplished by combining some bands. Therefore, this method did not apply to this study area due to high vegetation. Sabin's Ratio (band 4/2, 6/7, and 6/5), Kaufmann's Ratio (band 7/5, 5/4, 6/7), and composite of band 4/2, 6/7, 5 were also examined as shown in Figure 4.

Advanced analysis was conducted using PCA andpotential mineral zones were visible. Based on eigenvalue and eigenvector calculations, PC1, PC2, and PC3 possessed data variance of more than 99.83% in RGB format. The dark blue and green tint sections showed possible mineral zones and flora, respectively. Meanwhile, the bright pixels represented hydrothermally altered rocks in Figure 5B. Figure 7 shows that mineral zones from PCA method were located as drill holes and yellow dots were drill holes from the previous study. Dark blue zones were potential mineral areas and the green boxes were the suggested exploration areas.

In conclusion, While the Band Ratios method did not effectively distinguish mineral zones due to the presence of dense vegetation, the PCA method demonstrated significant potential. The application of PCA to the spectral bands revealed distinct variations that could be attributed to mineral zones, even in areas with substantial vegetation cover. Key findings from the PCA analysis include:

1. Principal Components Analysis (PCA):
2. Over 99.83% of the variance in the data was explained by the first three principal components (PC1, PC2, and PC3) taken together. Indicating that these components captured the most critical information from the spectral bands.
3. The fourth principal component (PC4) identified bright pixels corresponding to hydrothermally altered rocks, providing a clear distinction from vegetative cover.

These results suggest that PCA could enhance the accuracy and clarity of mineral zone identification. This approach offers a promising avenue for future research, particularly in areas with complex surface conditions. The integration of the method with machine learning might produce clearer differences for potential zones.

References

Aita, S. K., and A. E. Omar (2021), Exploration of uranium and mineral deposits using remote sensing data and GIS applications, Serbal area, Southwestern Sinai, Egypt, *Arabian Journal of Geosciences*, *14*(21), https://doi.org/10.1007/s12517-021-08568-0.

Bakardjiev, D., and K. Popov (2015), ASTER spectral band ratios for detection of hydrothermal alterations and ore deposits in the Panagyurishte Ore Region, Central Srednogorie, Bulgaria, *Review of the Bulgarian Geological Society*, *76*(1), 79–88.

Burrows, D. R., M. Rennison, D. Burt, and R. Davies (2020), The Onto Cu-Au Discovery, Eastern Sumbawa, Indonesia: A Large, Middle Pleistocene Lithocap-Hosted High-Sulfidation Covellite-Pyrite Porphyry Deposit, *Economic Geology*, *115*(7), 1385–1412, https://doi.org/10.5382/econgeo.4766.

Carranza, E. J. M., and M. Hale (2002), Mineral imaging with Landsat Thematic Mapper data for hydrothermal alteration mapping in heavily vegetated terrane, *International Journal of Remote Sensing*, *23*(22), 4827–4852, https://doi.org/10.1080/01431160110115014.

Chen, Q., Z. Zhao, J. Zhou, et al. (2021), New Insights into the Pulang Porphyry Copper Deposit in Southwest China: Indication of Alteration Minerals Detected Using ASTER and WorldView-3 Data, *Remote Sensing*, *13*(14), 2798, https://doi.org/10.3390/rs13142798.

Fadlin, R. Takahashi, A. Agangi, et al. (2023), Geology, mineralization and calcite-rich potassic alteration at the Humpa Leu East (HLE) porphyry Cu-Au prospect, Hu'u district, Sumbawa Island, Indonesia, *Resource Geology*, *73*(1), https://doi.org/10.1111/rge.12309.

Ghasemi, K., B. Pradhan, and R. Jena (2018), Spatial Identification of Key Alteration Minerals Using ASTER and Landsat 8 Data in a Heavily Vegetated Tropical Area, *Journal of the Indian Society of Remote Sensing*, *46*(7), 1061–1073, https://doi.org/10.1007/s12524-018-0776-0.

Hede, A. N. H., K. Kashiwaya, K. Koike, and S. Sakurai (2015), A new vegetation index for detecting vegetation anomalies due to mineral deposits with application to a tropical forest area, *Remote Sensing of Environment*, *171*, 83–97, https://doi.org/10.1016/j.rse.2015.10.006.

Ombiro, S. O., A. S. Olatunji, E. M. Mathu, and T. R. Ajayi (2021), Application of remote sensing in mapping hydrothermally altered zones in a highly vegetative area - A case study of Lolgorien, Narok County, Kenya, *Indian Journal of Science and Technology*, *14*(9), 810–825, https://doi.org/10.17485/IJST/v14i9.68.

Parcutela, N. E., C. B. Dimalanta, L. T. Armada, et al. (2022), Band processing of Landsat 8-OLI multi-spectral images as a tool for delineating alteration zones associated with porphyry prospects: A case from Suyoc, Benguet, Philippines, *IOP Conference Series: Earth and Environmental Science*, *1071*(1), 012,022, https://doi.org/10.1088/1755-1315/1071/1/012022.

Pour, A. B., and M. Hashim (2014), Alteration mineral mapping using ETM+ and hyperion remote sensing data at Bau Gold Field, Sarawak, Malaysia, *IOP Conference Series: Earth and Environmental Science*, *18*, 012,149, https://doi.org/10.1088/1755-1315/18/1/012149.

Setianto, A., B. Raharja, and A. D. Titisari (2021), Application of Landsat 8 Image in An Assessment of Hydrothermal Alteration Mapping in Dense Vegetation: A Case Study from Kokap Area, Kulon Progo, *Indonesian Journal on Geoscience*, *9*(1), 45–60, https://doi.org/10.17014/ijog.9.1.45-60.

Shebl, A., and A. Csámer (2021), Lithological, structural and hydrothermal alteration mapping utilizing remote sensing datasets: a case study around Um Salim area, Egypt, *IOP Conference Series: Earth and Environmental Science*, *942*(1), 012,032, https://doi.org/10.1088/1755-1315/942/1/012032.

Shim, K., J. Yu, L. Wang, et al. (2021), Content Controlled Spectral Indices for Detection of Hydrothermal Alteration Minerals Based on Machine Learning and Lasso-Logistic Regression Analysis, *IEEE Journal of Selected Topics in Applied Earth Observations and Remote Sensing*, *14*, 7435–7447, https://doi.org/10.1109/JSTARS.2021.3095926.

Takodjou Wambo, J. D., S. Ganno, N. A. Afahnwie, et al. (2016), Use of Landsat 7 ETM + Data for the Geological Structure Interpretation: Case Study of the Ngoura-Colomines Area, Eastern Cameroon, *Journal of Geosciences and Geomatics*, *4*(3), 61–72, https://doi.org/10.12691/jgg-4-3-3.

Verdiansyah, O., A. Idrus, L. D. Setijadji, B. Sutopo, and I. G. Sukadana (2021), Mineralogy of hydrothermal breccia cement of Humpa Leu East porphyry copper-gold prospect, Sumbawa Island, Indonesia, *E3S Web of Conferences*, *325*, 04,008, https://doi.org/10.1051/e3sconf/202132504008.

Verdiansyah, O., A. Idrus, L. D. Setijadji, B. Sutopo, and I. G. Sukadana (2023), Elemental mapping and mineral distribution of the Humpa Leu East porphyry samples: An implication to understand the pattern of mineralization, in *4TH INTERNATIONAL CONFERENCE ON EARTH SCIENCE, MINERAL AND ENERGY*, vol. 2598, p. 020008, AIP Publishing, https://doi.org/10.1063/5.0126120.

Zhang, T., G. Yi, H. Li, et al. (2016), Integrating Data of ASTER and Landsat-8 OLI (AO) for Hydrothermal Alteration Mineral Mapping in Duolong Porphyry Cu-Au Deposit, Tibetan Plateau, China, *Remote Sensing*, *8*(11), 890, https://doi.org/10.3390/rs8110890.